Pergamon

Int. J. Heat Mass Transfer. Vol. 39, No. 16, pp. 3401–3415, 1996

0017-9310/96 $15.00+0.00

PII: S0017-9310(96)00026-9

Phase-resolved measurements in a gas-injected liquid bath

H. TURKOGLU† and B. FAROUK‡

Mechanical Engineering and Mechanics Departments, Drexel University, Philadelphia, PA 19104, U.S.A.

(*Received* 7 *August* 1995 *and in final form* 29 *November* 1995)

Abstract—The local phase volume fraction, bubble frequency, bubble velocity and phase resolved temperature distributions were measured in vertical air-injected water and air-injected multifluor™ inert fluid baths under different injection conditions. An electroresistivity probe was employed for determination of the local volume fraction, bubble arrival frequency and bubble velocity. The phase resolved temperatures were measured using a microthermocouple. The phase resolved temperature measurements are reported for the first time in these types of flow systems. The measurements showed that in the region close to the injection point, the gradients of the flow variables exhibit steep changes in radial and axial directions.

INTRODUCTION

The injection of gas jets into liquid baths has been practised commonly in metallurgical and chemical processing operations. Submerged gas injection has been used for the purpose of ferroalloy production, metal extraction and refining processes. These applications of the gas injection systems have resulted in the requirement for understanding flow structures and temperature fields in these systems. Flow in gas injected liquid baths is two-phase, highly turbulent and highly nonuniform. The mathematical formulation of such flows and interfacial heat transfer is not yet well established. Experimental data is needed to understand the structure of the flow and improve its mathematical representation.

It has been recognized that bubble formation at the nozzle exit, phase volume fraction, local bubble frequency and bubble rise velocity distributions in the gas–liquid plume region are important parameters in determining the characteristics of the system. The structure of the flow in the two-phase gas liquid region is of interest because the contacting pattern between the phases controls the interfacial area and hence, the physical and chemical processes taking place between the phases. The flow regime in the two phase region governs the overall flow in the liquid and hence the mixing intensity. After injection, the gas expands rapidly into a cone and a gas–liquid plume forms. The structure of this two-phase plume has been characterized in terms of gas concentration, bubble frequency and bubble velocity. Experiments have been carried out in air–water systems using electroresistivity probes [1–7].

In gas injection systems, the gas temperature at the nozzle exit is usually different from the liquid temperature. Hence, after the gas is discharged into the liquid, the phases exchange heat to reach thermal equilibrium. Heat transfer between the phases near the injection point plays important roles in the nozzle operation. The rate of the thermal expansion of the gas and the bubble/jet formation at the nozzle exit are also affected by the heat transfer mechanism between the phases. Accretion (solid finger-like outgrowths) formation in molten metal baths at the nozzle exit depends on the heat transfer mechanism between the phases. The shape and size of the accretions depend on the heat transfer between the injected gas and the molten metal. Accretion formation has been the subject of studies involving measurements and mathematical models [8–11]. Detailed temperature measurements have not been carried out to characterize the heat transfer mechanism between the phases in such systems.

A large number of measurement techniques for two phase flows have been developed and used by design engineers and investigators. Experimental methods for investigation of average flow parameters and local statistical characteristics of two-phase flows have been developed. Jones and Delhaye [12], Delhaye [13] and Hewitt [14] give a critical review of the measurement techniques and difficulties encountered in two-phase flow measurements. For volume fraction, bubble frequency and bubble velocity measurements, electroresistivity probe, optical probes and hot wire/film anemometer have been used by different researchers [2–4, 7, 15–17, 19]. Glass rod [20], fibre bundle [21], and U shaped fibre systems have also been used. Measurements with hot-wire anemometers were reported by Shiralkar and Lahey [22] and Delhaye [23], among others.

† Present address: Department of Mechanical Engineering, Gazi University, Ankara, Turkey.

‡ Author to whom correspondence should be addressed.

NOMENCLATURE

A	surface area of the thermocouple bead
a	filter coefficient
C_p	specific heat of the thermocouple substance
D	diameter of the thermocouple bead
f_B	bubble frequency
h	heat transfer coefficient
k	thermal conductivity
m	mass of the thermocouple bead
N	total number of bubbles detected in a data record
Pr	Prandtl number
R_g	time averaged gas volume fraction
Re	Reynolds number based on the thermocouple bead diameter and gas/liquid properties
r	radial distance from the axis of the vessel
t	time
t_g	residence time of a bubble at the probe tip
T	temperature
T_c	temperature of the continuous phase
T_d	temperature of the dispersed phase
x	input to the digital filter
X	binary variable representation of the phase signals
y	output from the digital filter
z	axial distance from the injection point.

Greek symbols

τ	total sampling time for a data record
τ_g	total time during which a point (probe tip) is occupied by the gas phase in a data record
τ_c	thermocouple time constant in the continuous phase
τ_d	thermocouple time constant in the dispersed phase.

Subscripts

c	continuous phase
d	dispersed phase.

Microthermocouples have been used for the measurement of the phase temperatures in two-phase flows. A review of studies on temperature measurements in two-phase flows using microthermocouples is given by Jones and Delhaye [12] and Hewitt [14]. Experiments have been carried out on boiling heat transfer to study temperature fluctuations near a heated surface with either pool boiling or forced convection. Marcus and Dropkin [24] used a microthermocouple probe made up of wires 50 μm in diameter in measuring mean fluctuating temperatures to evaluate the thickness of the superheated layer in contact with a heated wall. Van Stralen and Sluyter [25] performed experiments to characterize temperature fluctuations and growth of bubbles generated at a heating strip in a test section. Stefanovic *et al.* [26] used a 40 μm diameter thermocouple and obtained amplitude histograms in pool boiling and in forced convection boiling. The authors separated steam and water temperature histograms by assuming that the predominant phase had a symmetrical temperature distribution. Similar measurements were performed by Afgan *et al.* [27]. Superheated layer thickness measurements were conducted in saturated and subcooled nucleate boiling by Wiebe and Judd [28] using a 75 μm chromel–constantan and microthermocouple. A time averaged temperature was determined by integrating the temperature signal.

The preceding works have contributed to a large extent to the understanding of the local thermal structure of two-phase flows. However, no phase-resolved temperature measurements for the gas-injected liquid bath systems were obtained. In the present paper, phase volume fraction, bubble frequency, bubble velocity and phase resolved temperature measurements are reported for air-injected water and air-injected multifluor™ inert† fluid baths. Measurements were carried out in water and multifluor inert fluid baths contained in a cylindrical vessel. A stream of air was injected through a vertical nozzle located centrally at the bottom of the vessel. In the air/water systems, the local values of the gas volume fraction, bubble frequency, bubble velocity, and phase temperatures were measured. In the air/multifluor inert fluid systems, only the phase temperatures were measured since multifluor inert fluid is not electrically conductive. An electroresistivity probe was employed for the determination of the local void fraction and bubble arrival frequency. A double contact electroresistivity probe was used for the measurement of bubble velocity. Both cold air/hot water and hot air/cold water systems were used for temperature measurements. For the multifluor inert fluid, only hot air jets were used. The phase resolved temperatures were measured using a microthermocouple. A digital filtering and time response compensation technique were applied to the microthermocouple signals.

EXPERIMENTAL APPARATUS

In the present study, measurements were performed in vertical gas injected liquid baths. The apparatus

† Multifluor inert liquid is a trademark of Air Products and Chemicals, Inc.

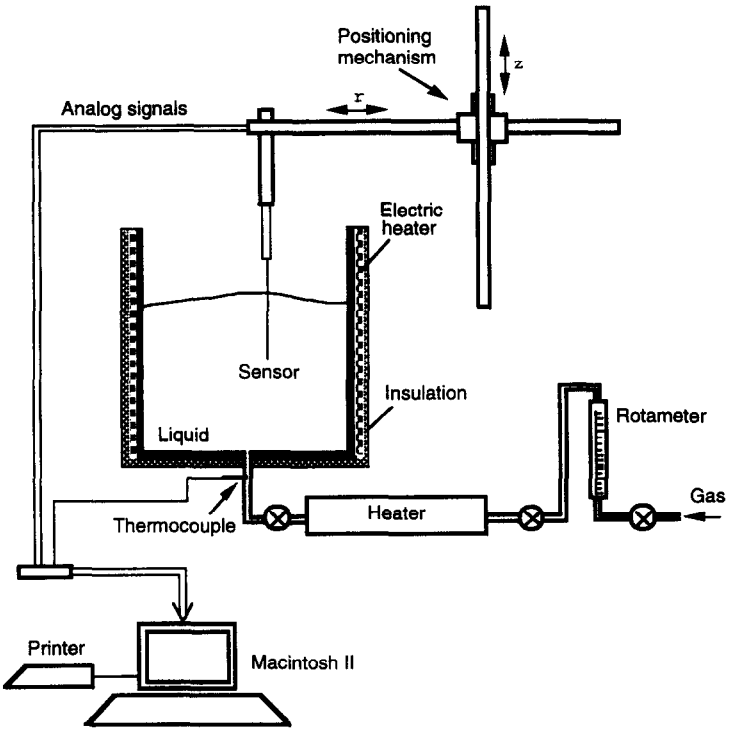

Fig. 1. Schematic diagram of the experimental facility.

employed is illustrated schematically in Fig. 1. The individual components can be divided into four main subsystems: (1) the cylindrical vessel, (2) the heater and the gas delivery system, (3) the probes and positioning mechanism and (4) the data acquisition system. An oscilloscope (Norland Corp., Prowler) and a digital thermometer (Omega Engineering, Inc., Digicator) were used as supporting equipment.

The cylindrical vessel containing the liquid was built by flanging a Pyrex-glass tube to a stainless steel plate. The vessel had an internal diameter of 300 mm and a height of 200 mm. The injection nozzle was located centrally at the bottom of the vessel. The nozzle was machined from a Teflon rod and had a straight inner hole 1.58 mm in diameter. The outside diameter was 25.4 mm and threaded so that it could be screwed into the threaded hole in the bottom plate flush with the inner surface of the plate. A thermocouple was installed 35 mm upstream of the nozzle exit to monitor the temperature of the gas before it discharges into the liquid. An electric tape heater of 800 kW was installed around the vessel to heat the liquid in the vessel (when needed). The heater was controlled with a digital temperature controller (Omega Engineering, Inc., CN310) to maintain the liquid temperature at a desired level. All faces of the vessel were then insulated except the top surface which was open to the atmosphere.

Injection air was supplied by a central compressor in the laboratory. The gauge pressure of the air line was 620.5 kPa. A pressure regulator and filter were used at the entrance of the system. The gas flow rate was monitored using a rotameter with a spherical float (Emerson Electric, Co., R615B). Two needle valves and pressure gages were placed at the entrance and exit of the rotameter. The air exiting from the rotameter passed through the heater which was made of a 25.5 mm diameter stainless steel flexible tube and a 2400 kW electric heater tape. The bubble sizes ranged from 2–10 mm for the flow rates considered in the study. The temperature of the air at the exit was controlled by a temperature controller (Omega Engineering, Inc., CN310). The heater exit was connected to the injection nozzle through a two-branch tubing arrangement. A three-way solenoid valve was connected to one branch and a needle valve was placed on the other branch. This arrangement provided a means to direct part of the gas to the environment, if needed, at the beginning of the experiments.

A two-dimensional positioning mechanism was built to locate the probes accurately (± 0.02 mm) at the measurement points within the flow domain. The mechanism was constructed from two linear unislides (Velmex, Inc., A1518Q2). The location of the probe tips was determined using the scales placed on both the vertical and horizontal slides of the mechanism. The data acquisition system consisted of a plug-in board (MacADIOS II, GW Instrument, Inc.) and a Macintosh II computer.

Ideally, a single probe that measures temperature and can distinguish phases is desirable. An attempt to obtain data by positioning a phase sensor (electroresistivity probe) and a microthermocouple in close proximity was not successful. This was primarily due

to the interference of the electroresistivity probe on the microthermocouple signal. Hence, gas volume fraction and phase resolved temperature measurements were performed sequentially. The temperature of each phase was determined from a single thermocouple data record. When the injected gas was colder than the liquid in the bath, it could be assumed that at any point in the flow domain the temperature of the gas was always less than or equal to the liquid temperature. This information can be used to identify whether a point on a temperature signal trace was taken in the gas or liquid phase. In the systems studied, some prior qualitative information about the phase temperatures was available. Further details of the experimental procedure can be found in ref. [29].

An electroresistivity probe with a single sensor was used for the gas volume fraction and bubble frequency measurements. For the velocity measurements, a double contact electroresistivity probe was employed. Tips of the double contact electroresistivity probe was on the same vertical line and 2 mm apart from each other. The sensing elements were made from stainless steel and were soldered to a length of copper wire. The entire surface of the needles was coated with a thin layer of red Glpt insulating varnish (marketed by G. C. Electronics). The Glpt coating was dissolved from the tip of the needles using Strip-X (a solvent marketed by G. C. Electronics) leaving a 0.1 mm long bare tip measuring 0.1 mm at its largest diameter. These dimensions were chosen following suggestions of Castillejos [30]. The wire was then passed through a ceramic insulating tube which was housed in a stainless steel support tube. Both ends of the stainless steel sheath were sealed with epoxy resin to prevent any infiltration of the liquid. The bottom plate of the vessel was employed as the return (reference) electrode. A direct current power supplier (~ 5 V) was used to energize the circuitry so that voltage pulses between the sensing element and the return electrode could be measured. To minimize the current flow, an external resistor of 500 kΩ was placed into the circuitry in series.

The probe used for the phase resolved temperature measurements was a chromel–constantan (E type) microthermocouple. The microthermocouple, made from 25 μm wires, was welded to lead wires which were 0.127 mm in diameter. The wires were then passed through a two-hole ceramic insulating tube. Only a small length of the microthermocouple (~ 2 mm) was outside the ceramic tube. Both ends of the ceramic tube were carefully sealed with epoxy-resin. To increase the rigidity of the microthermocouple, the epoxy-resin was extended toward the hot junction (bead), but it was made sure that the hot junction was bare. The ceramic tube was then placed in a stainless steel sheath. Both ends of the steel case were sealed to prevent any liquid infiltration. The extension wires were shielded with aluminium foil up to the analog break out (ABO) unit to reduce the effects of electronic noise on the signals.

SIGNAL ANALYSIS

Analysis of the electroresistivity probe signal

Figure 2 shows an idealized and a real phase signal traces. The ideal signal trace [Fig. 2(a)] was drawn from the principles of the electroresistivity probe. If the tip of the sensor ideally pierces the bubbles, the signal would be a sequence of rectangular pulses, each representing a bubble. The length of the pulses corresponds to the time during which the tip of the probe is in the gas phase. Since, the bubbles arrive in an irregular manner, the length and frequency of the pulses are random, as seen in Fig. 2(b). This makes it necessary to examine the state of the bubble contacts continuously with a computer to extract information on the behavior of the bubbles. This requires conversion of the analog into digital signals prior to analysis. The digital signal can then be analyzed on the basis of the definition of the flow parameters to be measured (local gas volume fraction and bubble frequency). Using a voltage threshold level, the analog signals can be approximated with a binary variable, $X(x, t)$, which is a function of position and time. $X(x, t)$ is unity when the probe tip is in the liquid phase, and $X(x, t)$ is zero when the tip is in the gas phase. Selection and effects of the threshold voltage on the measured parameters are discussed in detail by Turkoglu [29].

The local gas volume fraction (or rather local gas time fraction) is defined as the probability of the existence of the gas phase at a given point. Under steady state conditions, the time averaged local 'gas time fraction' is given by

$$R_G(\mathbf{x}) = \frac{1}{\tau}\int_0^\tau X(\mathbf{x}, t)\,dt = \frac{\sum_{n=1}^{N} t_{G,n}}{\tau} = \frac{\tau_G}{\tau}, \qquad (1)$$

where $t_{G,n}$ is the contact time of the probe with the bubble n, τ is the total sampling time, and N is the total number of bubbles that pass through the probe tip during the time period τ. This method for the determination of the gas fraction is valid if the sampling time is sufficiently long to allow statistical treatment of the signals. It has been theoretically proven [31] that the local 'gas time fraction' and the local gas volume fraction are identical quantities. Hence, in this work, hereafter 'time fraction' and 'volume fraction' are considered to be identical as far as the measurements are concerned, and only 'volume fraction' is used in the text.

The local bubble frequency is defined as the rate of arrival of the bubbles at a point (probe tip) in the flow domain. Each pulse in the signal traces obtained from the electroresistivity probe represents a bubble. The total number of bubbles, N, arriving at the probe tip for a given duration τ can be determined from these signals. Then the local bubble frequency is calculated as

$$f_B = \frac{N}{\tau}. \qquad (2)$$

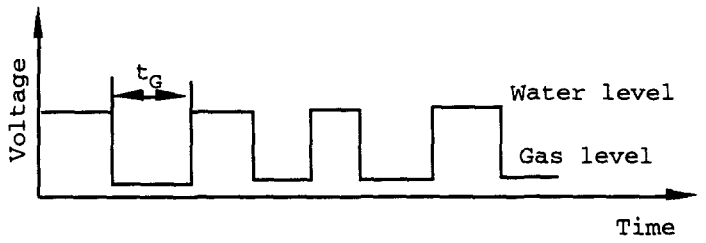

(a)

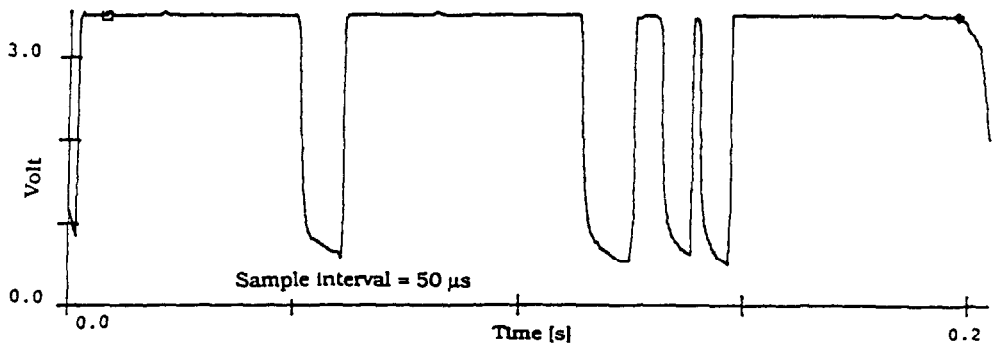

(b)

Fig. 2. Idealized and real signal traces obtained from the electroresistivity probe. (a) Ideal signal, (b) real signal.

A modified form of the probe was used for the bubble velocity measurements, as explained earlier. The bubble rise velocity is determined using the signals obtained from both tips of the electroresistivity probe. The time taken by the bubbles to travel from the lower tip of the probe to the upper tip is figured out from these signal traces. Then, the velocity is calculated as the ratio of the vertical distance between the probe tips to the time period taken by a bubble to rise from the lower tip of the probe to the upper tip.

Analysis of temperature signals

The thermocouple placed in the gas–liquid plume is randomly hit by bubbles rising in the liquid. The same thermocouple senses both the gas and the liquid phase temperatures at the same point. However, at any given instant, it can only sense the temperature of the phase surrounding it. Thus, the thermocouple provides a quasi-periodic sequence of information on the temperature of the phases. The same signal trace contains information from both phases. The phase-resolved temperature measurements involved determination of the temperature of each phase from the same signal trace.

An idealized (hypothetical) and a filtered and compensated real temperature trace (for cold gas injection into hot water) are given in Fig. 3(a) and (b), respectively. Similar to the phase signals, the temperature signals also consist of two levels, each representing the temperature of one phase. However, transition from one level to the other is not as sharp as in the phase signals [see Fig. 2(b)] due to temperature gradient on both sides of the interface and the longer response time of the thermocouple. This situation is depicted in Fig. 3(a).

The thermocouple signals are, in general, low in amplitude (of the order of millivolts). This makes them quite sensitive to the electrical noise generated by power lines, electronic equipment, radio waves, etc. Unless this noise is filtered out effectively, the measurements are not meaningful. In some systems, the residence time of the phases at the probe tip may be less than the response time of the thermocouple. In such cases, the thermocouple temperature cannot reach the temperature of the phase surrounding the hot junction. Hence, in order to obtain the phase temperatures from the thermocouple temperatures, a correcting operation (compensation) should also be performed.

Digital filtering of temperature signals

To obtain statistically meaningful phase temperatures, the noise superimposed on the temperature sig-

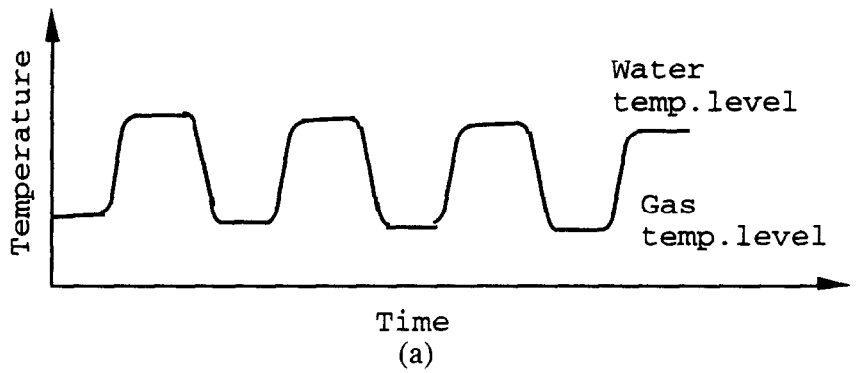

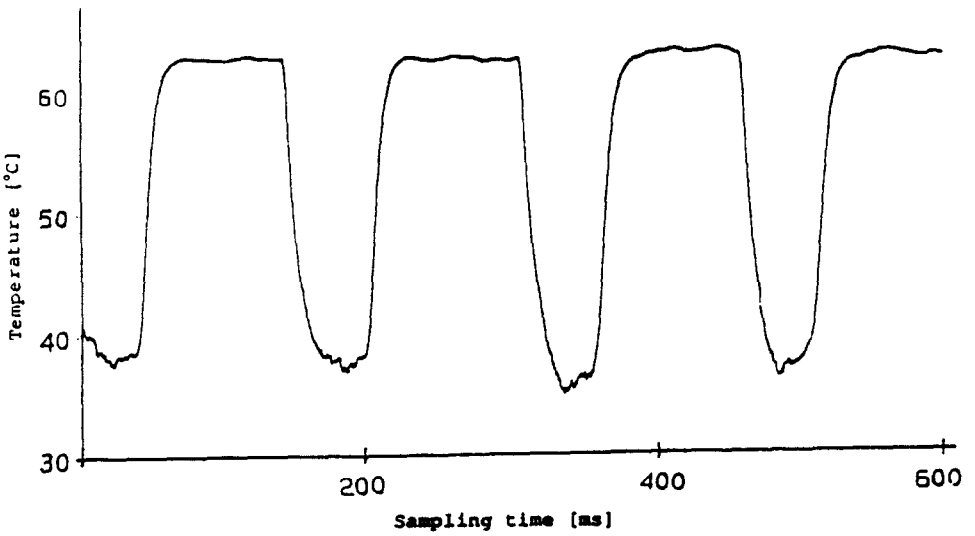

(b)

Fig. 3. Ideal (a) and real (b) thermocouple signal traces.

nals must be removed. In the present study, a low pass digital filter was used to filter the signals. The filter was defined by [32]

$$y_n = ax_n + (1-a)y_{n-1}, \tag{3}$$

where x_n is the input, y_n is the output, and a is the filter coefficient. The value of a ranges between zero and one.

Compensation for the thermocouple response

Thermal inertia causes the temperature of the thermocouple to lag behind that of the fluid surrounding the bead with a reduced amplitude. Hence, the thermocouple temperatures must be corrected to obtain the temperatures of phases. With perfect compensation, it is theoretically possible to recover the phase temperatures from those measured [33].

Thermocouple compensation techniques have been widely used in temperature measurements within turbulent flames to investigate the temperature fluctuations. Researchers have used either electrical or digital compensation techniques. Although the electrical compensation has been proven useful, it has severe limitations [34]. The most significant limitation is that, as the value of 'time constant' increases, the maximum frequency that might be compensated accurately decreases substantially because of the increased electrical noise from the compensator. Digital compensation overcomes many of the limitations of the electrical compensation; the noise level is reduced because fewer electronic components are used, and the digital compensation is more flexible and is generally more accurate. Digital signal processing also simplifies the procedure of applying additional corrections to the temperature data, such as radiation heat transfer, and conduction heat transfer to the leads, if needed. Another advantage is that various time constants may be used to compensate the same temperature data without resampling.

In the present work, a digital compensation tech-

nique was used. The thermal lag between the temperatures of the phases and thermocouple junction can be analyzed by a lumped capacity method [35]. This yields

$$T_c(t) = T(t) + \tau_c \frac{dT(t)}{dt} \tag{4}$$

for the continuous phase and

$$T_d(t) = T(t) + \tau_d \frac{dT(t)}{dt} \tag{5}$$

for the dispersed phase, where $T_c(t)$, $T_d(t)$ and $T(t)$ are the temperatures of the continuous phase, dispersed phase, and the thermocouple, respectively. Here τ_c and τ_d are the time constants of the thermocouple in the continuous and the dispersed phases, respectively. These are calculated as

$$\tau_c = \frac{mC_p}{h_c A} \quad \text{and} \quad \tau_d = \frac{mC_p}{h_d A}. \tag{6}$$

The time constants depend on the size of the bead and properties of the thermocouple material (mass m, specific heat C_p), and the heat transfer coefficients (h_c or h_d) between the thermocouple bead and the surrounding phase. If τ_c and τ_d are known, then equations (4) and (5) provide the necessary tools to determine the corrected phase temperatures from the thermocouple temperature.

Usually, an average time constant is used for compensation. An instantaneous time constant has been used for the measurements of the temperature fluctuations in premixed flames [36, 37]. Use of variable time constants involves the simultaneous measurements of temperature and velocity. Although the instantaneous compensation of the thermocouple measurements is possible, the expected small increase in accuracy may not justify the added cost and complexity. The use of an average time constant greatly simplifies measurements and data reduction because additional simultaneous velocity measurements are not necessary, and the required number of calculations are significantly reduced. Cambray *et al.* [38] compared the instantaneous thermal inertia compensation using a two-wire method with that of using an average time constant. They found that, even in cases of large time constant fluctuations, compensation with an average time constant does not lead to significant differences. The average time constant may be measured *in-situ* by electrical heating methods [39, 40] or by the two-wire method [38]. Another technique to obtain the average time constant is via theoretical calculations [35, 41]. In the present study, the latter approach was adopted.

The heat transfer coefficients between the phases and the thermocouple bead were calculated using the correlation [42]

$$h = \frac{k}{D}(2.0 + 0.60 Re^{0.5} Pr^{0.3}), \tag{7}$$

where D is the sphere diameter of the thermocouple bead, and the physical properties are for the surrounding fluid. The bead diameter of the thermocouple used in the present study was 0.0584 mm.

The time constants in air, water and in multifluor inert fluid calculated using equations (6) and (7) are found to change very little for fluid velocities larger than 0.4 m s^{-1} [29]. The error introduced would be insignificant if an average time constant was used for higher fluid velocities. In order to apply equations (4) and (5) for phase-resolved temperature measurements, it must be known whether $T(t)$ is taken in the liquid phase or gas phase. The position of the liquid–gas interfaces must be found on the temperature signal trace. At the liquid–gas interface, the following conditions must be met: (1) the temperature is the same for both phases, and (2) the heat flux is continuous. That is, at the interface

$$T_c(t) = T_d(t) = T_{int}(t) \tag{8}$$

and

$$k_c \frac{\partial T_c}{\partial r} = k_d \frac{\partial T_d}{\partial r}. \tag{9}$$

From equations (4) and (5), it can be shown that at the interface

$$\tau_c \frac{\partial T(t)}{\partial t} = \tau_d \frac{\partial T(t)}{\partial t}. \tag{10}$$

Equation (10) implies discontinuities of the first derivatives of the thermocouple temperature at the interface. These discontinuities, however, did not show up directly in the collected data, due to the finite size of the thermocouple hot junction.

Due to this fact, an approach utilizing the prior qualitative information on the phase temperatures was used to find the liquid–gas interface. The derivative $dT(t)/dt$ in equations (4) and (5) was obtained numerically from the (filtered) temperature data records using a forward differencing scheme. The effect of compensation for the temperature measurements in the air–water systems was small [29]. However, for the air–multifluor inert fluid system, the discrepancy between the noncompensated and compensated signals was significant (up to 50%). The reason for this is that the time constant of the thermocouple in water is quite small ($\sim$0.5 ms) in contrast to that in multifluor inert fluid ($\sim$5.0 ms).

Determination of phase-resolved temperatures

The gas (dispersed phase) thermal conductivity is smaller than the liquid thermal conductivity. Hence, the thermal gradient on the liquid side of the interface would be small. The heat capacity of a gas bubble is quite small in comparison to that of the liquid surrounding it. The overall temperature change in the liquid will thus be very small for the present system. The above argument and the profile of the time–temperature traces suggest that local instantaneous phase

Table 1. Experimental conditions for the void fraction and bubble frequency measurements (isothermal air–water system)

Case	Orifice diameter [mm]	Vessel diameter [mm]	Bath depth [mm]	Gas flow rate Q [$Nm^3 s^{-1}$]	Gas velocity at nozzle exit, W_o [$m s^{-1}$]
1	1.58	300	150	0.646×10^{-4}	34
2	1.58	300	150	1.36×10^{-4}	71

temperatures are best represented by the local maxima and minima in the temperature signals. The local time averaged phase temperatures can then be obtained by averaging the local maxima and minima. Note that the average of the local maxima represents the local time averaged temperature of the hot phase, while the average of the local minima represents the local time averaged temperature of the cold phase. This approach reduces the effects of thermocouple response time and the unreliable determination of the interface temperature on the calculations of the phase temperatures.

EXPERIMENTAL RESULTS

Gas volume fraction measurements

The phase volume fraction measurements were carried out in air–water systems at gas flow rates of 0.646×10^{-4} and 1.36×10^{-4} $m^3 s^{-1}$ (25°C and 1 atm) as shown in Table 1. Assuming the flow in the bath to be axisymmetric, the measurements were performed on a vertical plane passing through the axis of the injection nozzle. At a given axial position on this plane, the measurements were performed radially on both sides of the axis. At each point, data were collected at a rate of 10 000 samples per second. The total sampling time changed from point to point between 20 and 50 s.

Typical results of the radial gas volume fraction profiles are plotted in Figs. 4 and 5 for Cases 1 and 2, respectively. Figure 5 shows the gas volume fraction profiles for only half of the vertical plane for Case 2. The time averaged gas volume fraction profiles are symmetrical about the axis of the injection nozzle and exhibit a Gaussian shape. The radial spread of the gas increases with the increasing axial distance from the

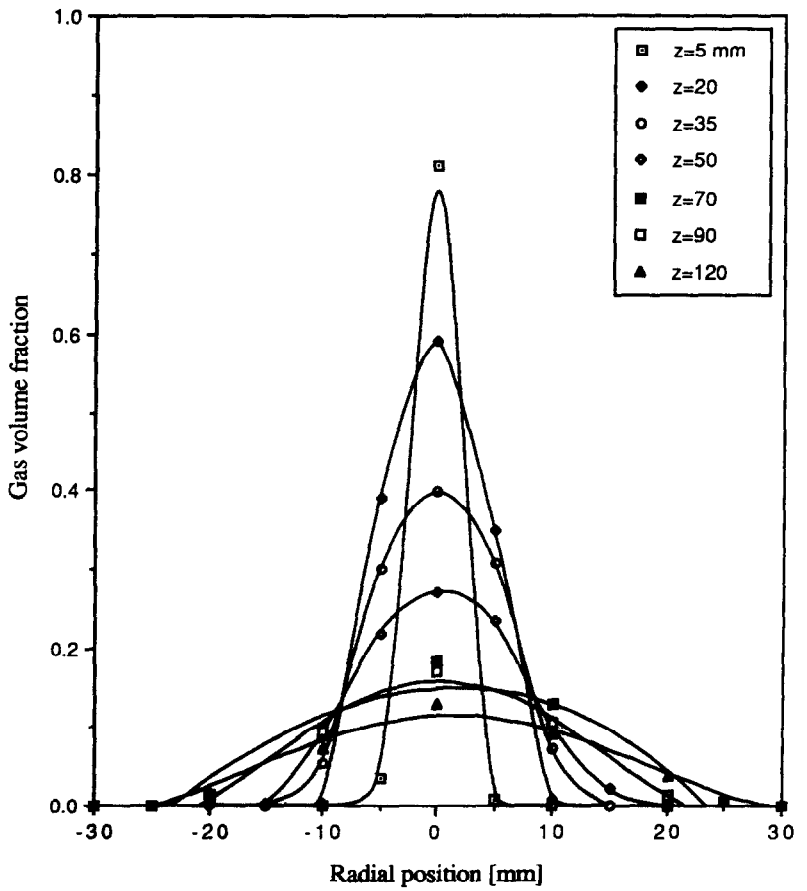

Fig. 4. Radial profiles of the gas volume fraction at different cross-sections, $Q = 0.646 \times 10^{-4}$ $Nm^3 s^{-1}$.

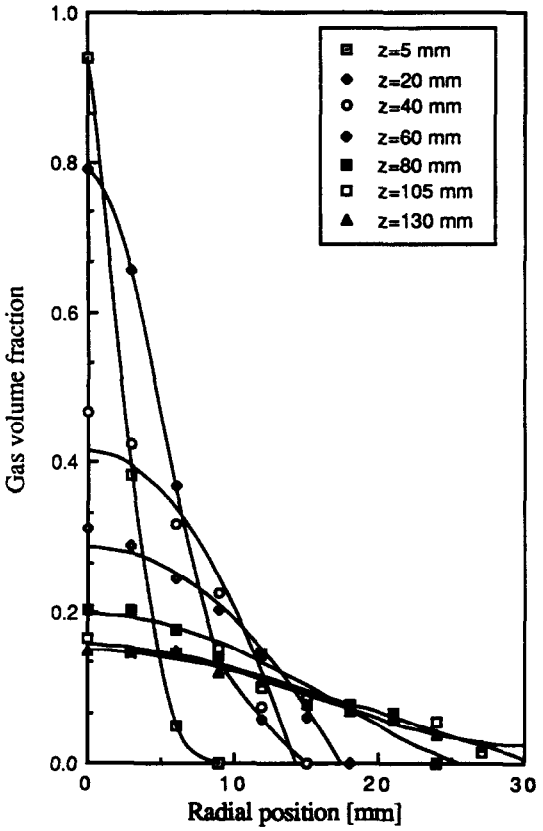

Fig. 5. Radial profiles of the gas volume fraction at different cross-sections, $Q = 1.36 \times 10^{-4}$ Nm^3 s^{-1}.

nozzle exit. The profiles become flatter away from the nozzle as more liquid is entrained by the gas bubbles into the rising plume. The profiles of the gas volume fraction along the axis of the nozzle are plotted in Fig. 6. This figure shows a rapid decrease in the gas concentration upon discharge and for $z > 70$ mm the volume fraction profiles are uniform.

The rapid decrease of the gas volume fraction indicates that the gas jet expands near the nozzle exit. The jet quickly entrains water and grows laterally. The gas concentration along the axis of the injection nozzle increases with increasing gas flow rate. A comparison of the radial gas volume fraction profiles on the horizontal plane at $z = 20$ mm is given in Fig. 7. This figure also shows that gas concentration along the axis of the injection nozzle increases with increasing gas flow rate. However, the radial dispersion of the gas plume does not show a considerable difference for the cases studied. This is in agreement with the findings of Castillejos [30]. His experiments in air–water systems, with different injection rates, showed that the cone angle of the gas–liquid plume changes from 18 to 22° with increasing injection rate. Visual studies carried out by Turkoglu [29] also showed that the gas concentration in the plume increases with increasing injection rate, however, the radial extent of the plume does not change considerably.

Bubble frequency profiles

Bubble frequency profiles are similar to gas volume fraction distributions in that they are also symmetrical and exhibit the same shape as the volume fraction profiles. The profiles become wider and flatter at the downstream of the injection point as the gas–liquid plume spreads radially. At high injection rates, a gas core region forms around the nozzle exit. The bubble break-up takes place away from this region. As a result, the local bubble frequency decreases and thereafter increases. A similar bubble break-up behavior was also observed by Castillejos and Brimacombe [4]. In general, with increasing axial distance, bubble frequency decreases as its radial dispersion increases.

Gas phase (bubble) velocity profiles

Radial profiles for the bubble velocities at different cross-sections are shown in Figs. 8 and 9 for Cases 1

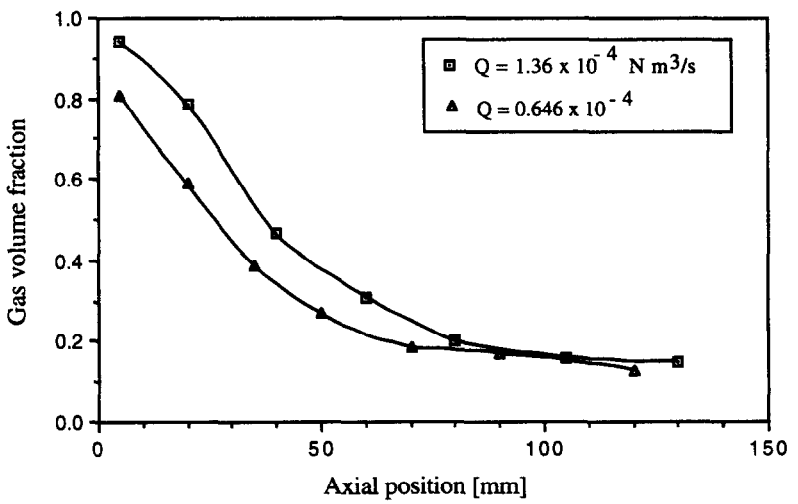

Fig. 6. Gas volume fraction profiles along the axis of the injection nozzle for two flow rates.

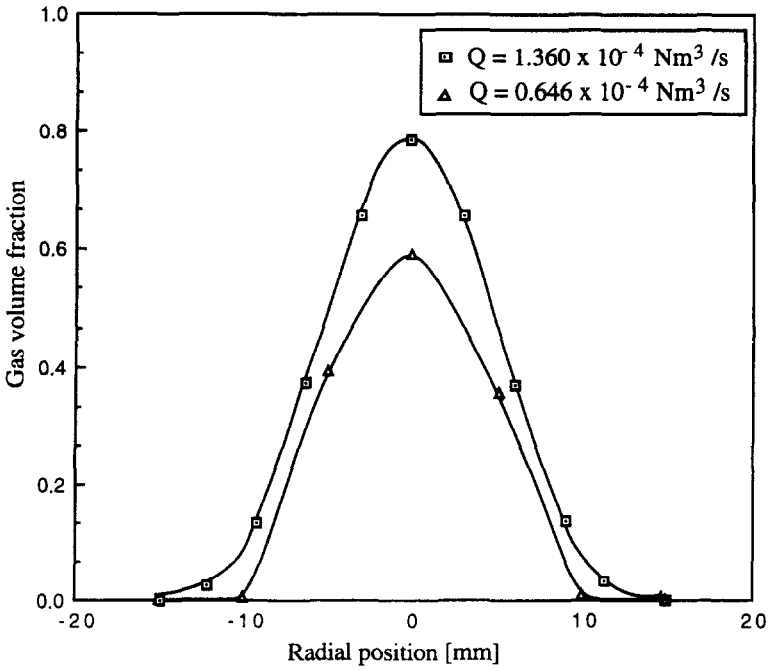

Fig. 7. Radial profiles of the gas volume fraction on horizontal plane at $z = 20$ mm for two flow rates.

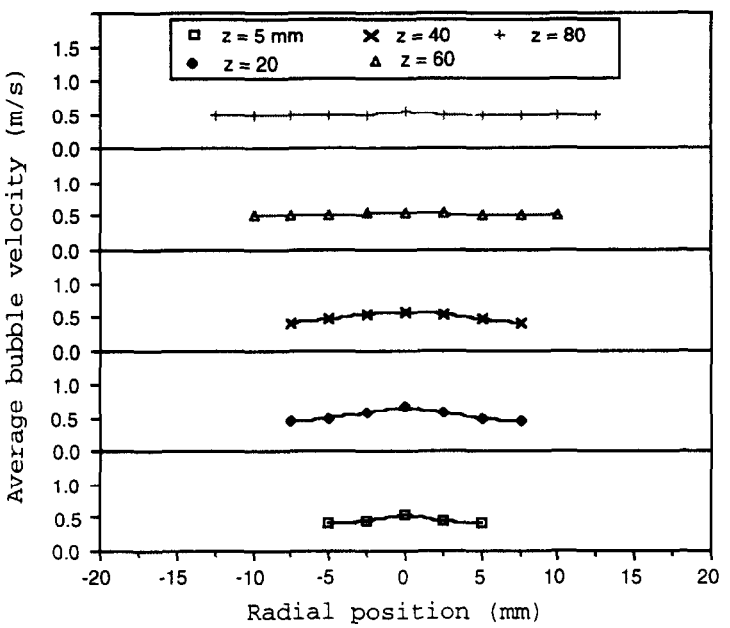

Fig. 8. Radial velocity profiles at different cross-sections, $Q = 0.646 \times 10^{-4}$ Nm^3 s^{-1}.

and 2, respectively. As seen, the velocity profiles are also symmetrical about the axis of the vessel and exhibit a normal distribution. Near the nozzle exit, it changes with the radial position as well as with the axial position. With further increase in the axial and the radial distances, the velocity profiles become flatter at a value around the terminal speed. The higher velocity in the high volume fraction region can be attributed to the wake effect observed in this region.

Phase temperature measurements

Phase resolved temperature measurements were carried out in vertical air–water and air–multifluor inert fluid systems. The vessel dimensions and liquid height in the vessel were the same as given in Table 1. The side and bottom walls of the vessel were thermally insulated; the top surface was open to the atmosphere. The measurements were carried out at different points along the axis of the injection nozzle in the two-phase

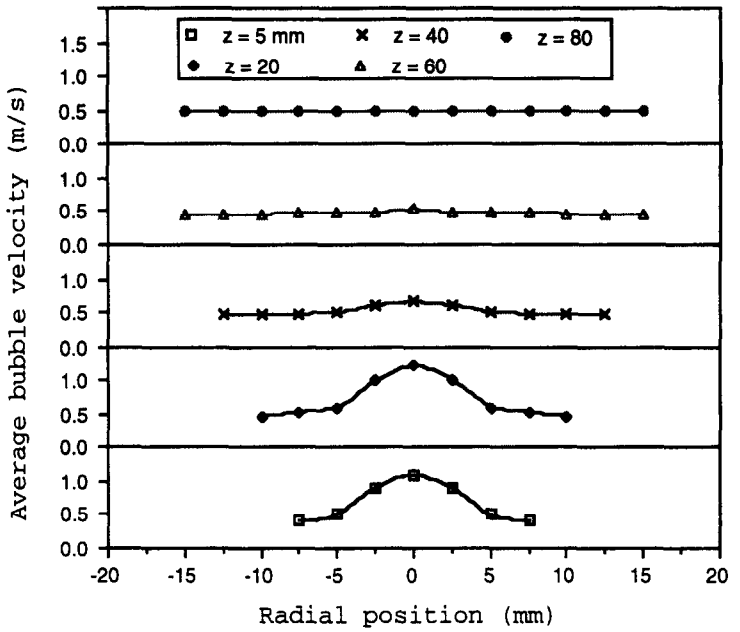

Fig. 9. Radial velocity profiles at different cross-sections, $Q = 1.36 \times 10^{-4}$ Nm^3 s^{-1}.

gas liquid region. The signals produced by the microthermocouple were analyzed to determine time averaged phase temperatures. Samples were collected at a rate of 10 000 per s for 5–10 s. The results of the measurements in air–water systems are presented first. Then, the results of the measurements in air–multifluor inert fluid systems are presented and discussed.

Temperature measurements in air–water systems

Measurements were carried out in both cold air–hot water and hot air–cold water systems. The experimental conditions for the temperature measurements in air–water systems are given in Table 2. For the case TW1, water in the bath was heated by a heater installed around the vessel. The temperature of the bath was kept at the predetermined value with a temperature controller. The measurement was started when a steady state initial bath temperature of 60°C was reached.

Temperature traces at different points along the axis indicated a two-level structure, each level representing the temperature of one phase. At points close to the injection nozzle, considerable differences between the upper and lower levels of the traces (between the phase temperatures) were observed. These differences decrease with increasing axial distance from the injection point. Finally, the air bubbles reach the water temperature, and the temperature trace becomes a straight line. It is observed that near the nozzle, the gas temperature is considerably different from the liquid temperature. It is also seen that near the nozzle exit, the water temperature changes from its initial value. However, away from the injection point, where the liquid concentration is high, the temperature change in the water is insignificant, since the amount of heat absorbed by the gas bubbles is small compared to the heat content of the water. The measurements on a given radius at points away from the axis did not show any difference between the phase temperatures. This could be attributed to the fact that the gas volume fraction decreases sharply with the radial distance from the axis of the injection nozzle (see Figs. 4 and 5). This indicates that the heat transfer between the phases is quite efficient when the phases are well mixed.

The results of the temperature measurements are presented in terms of normalized profiles, so that a comparison can be made between the temperature profiles obtained under different experimental conditions. The phase temperatures, T_i, are normalized as

$$\theta_i = (T_i - T_{\mathrm{L,intl}})/(T_{\mathrm{G,in}} - T_{\mathrm{L,intl}}),$$

Table 2. Experimental conditions for the temperature measurements in air–water systems

Case	Air flow rate Q [Nm^3 s^{-1}]	Initial bath temperature [°C]	Air inlet temperature [°C]
TW1	0.646×10^{-4}	60	24
TW2	0.646×10^{-4}	22	163.8
TW3	1.29×10^{-4}	22	182

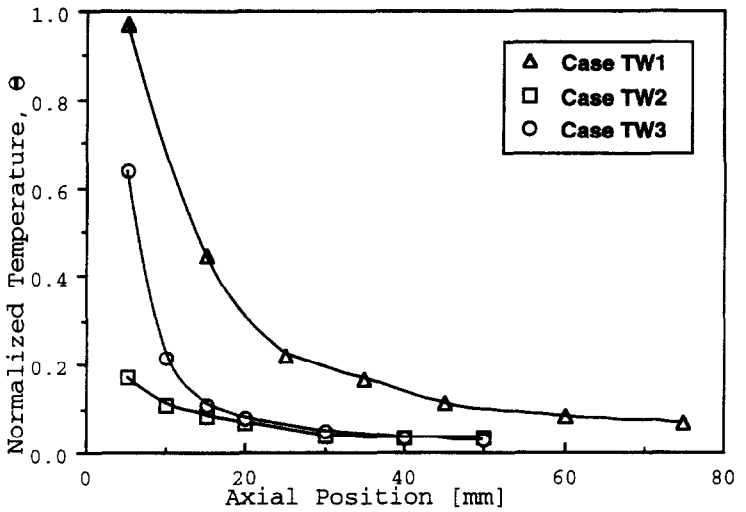

Fig. 10. Normalized gas temperature profiles along the axis of the injection nozzle for cases TW1, TW2 and TW3.

where $T_{L,intl}$ and $T_{G,in}$ are the initial liquid temperature and the gas temperature at the nozzle exit, respectively.

The normalized temperature profiles of the gas phase along the axis are plotted in Fig. 10, which shows that the liquid and gas have different temperatures around the nozzle exit, but reach equilibrium in a short distance thereafter. The extent of the region where the phases have different temperatures increases with increasing gas flow rate. The gas concentration in this region also increases with increasing injection rate. This indicates that the gas can maintain a temperature different from the liquid temperature over a larger distance from the injection point if the gas concentration is high.

Although a slight temperature change in the water near the nozzle exit is seen, considerable change in the bulk temperature of the water is not observed in the systems (TW2 and TW3) studied. This was also checked by a simple heat balance calculation as the experimental time was short (each experiment took 10–15 min). However, when a cold air stream was injected into the hot water bath (Case TW1), the bulk temperature of the liquid changed only 2–4°C. This was thought to be mainly due to heat transfer in the environment from the open top surface of the bath. Although the air temperature at the nozzle exit was higher than the boiling temperature of water (Cases TW2 and TW3), the temperature of the air and water in the bath were always lower than the boiling temperature. The maximum air and water temperature observed near the nozzle exit in the measurements performed were 88°C and 34°C (Case TW3, at $z = 5$ mm), respectively. When the distance from the injection point was increased, these temperatures dropped further.

The effect of local evaporation from the thermocouple surface could be important for the gas temperature measurements. For example, if an air bubble engulfing the thermocouple bead is not saturated with the water moisture, the liquid film on the bead will evaporate. As a result of this evaporation, the thermocouple cools down. This may result in a temperature reading lower than the bubble temperature. In the present experimental studies, no such cooling effect was expected. Even though air entering the heater is not saturated, its moisture content increases due to water draining into the gas line before it is discharged into the bath. As gas bubbles rise in the water, they pick up more moisture before reaching measurement locations. In the meantime, the air temperature decreases due to the heat transfer to the liquid phase.

Temperature measurements in air–multifluor inert fluid systems

The experiments in air–multifluor inert fluid systems were carried out in order to investigate the effects of the fluid properties on the heat transfer rate between the phases. Density, boiling temperature, thermal conductivity and specific heat of multifluor inert fluid are 2040 kg m^{-3}, 240°C, 0.067 J m^{-1} s^{-1} $°C^{-1}$ and 836 J kg^{-1} $°C^{-1}$, respectively. The measurements were performed under different injection conditions, keeping the bath sizes the same. A hot air stream was injected into the cold multifluor inert fluid bath. The injection conditions studied are given in Table 3.

The axial profiles of the normalized gas and liquid temperatures are plotted in Figs. 11 and 12, respectively. As shown, the temperature profiles in air–multifluor inert fluid systems exhibit a behavior similar to that seen in air–water systems. However, the changes in the phase temperature profiles are not as great as those observed in the air–water systems (see Fig. 10). Due to the low thermal conductivity and heat capacity of the multifluor fluid, the heat transfer rate between air and multifluor fluid is presumed to be less than that between air and water. As a result, the temperatures of

Table 3. Experimental conditions for the temperature measurements in air–multifluor inert fluid systems

Case	Air flow rate Q [Nm^3 s^{-1}]	Initial bath temperature [°C]	Air inlet temperature [°C]
TM1	0.323×10^{-4}	26	135
TM2	0.646×10^{-4}	21	135
TM3	1.29×10^{-4}	25	159

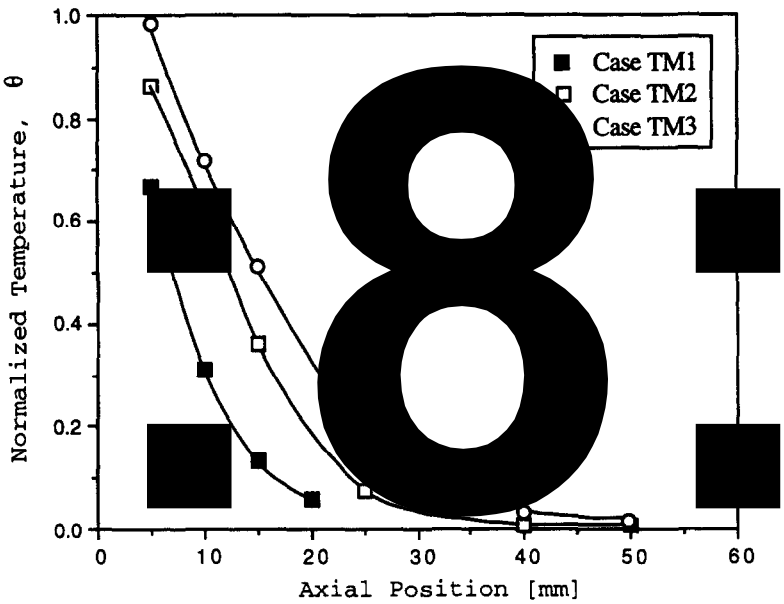

Fig. 11. Normalized gas temperature profiles along the axis of the injection nozzle for cases TM1,TM2 and TM3.

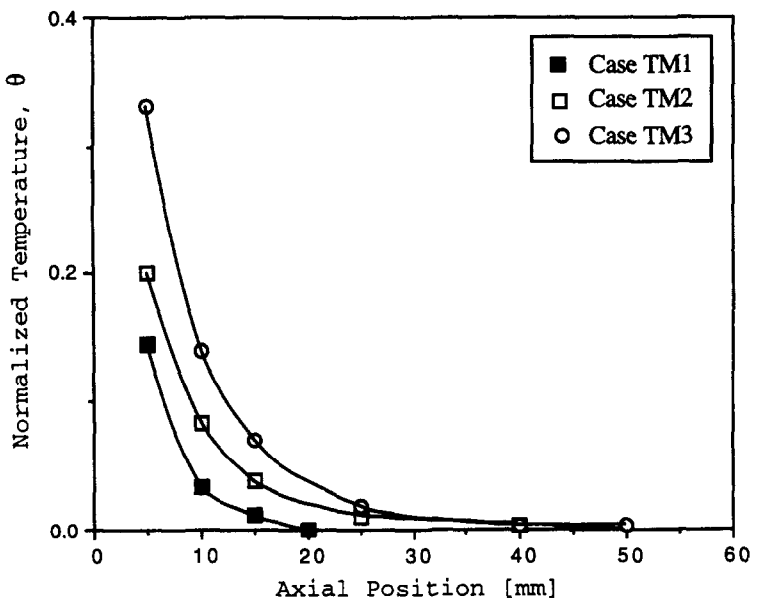

Fig. 12. Normalized liquid temperature profiles along the axis of the injection nozzle for cases TM1, TM2 and TM3.

the multifluor inert fluid and air become equal at longer axial distances (compared to the air–water cases) under the same operating conditions.

The results of these temperature measurements are of interest from both theoretical and practical points of view. The measurements have revealed that for the experiments performed, the phases reach an equilibrium temperature in a short distance from the injection point. Nevertheless, the phase temperatures near the nozzle exit are considerably different from each other. This indicates that when a cold gas stream is injected into molten metal baths, the temperature of the nozzle will be much less than the melt temperature due to the cooling of the injected gas. At high gas injection rates, the local cooling of the melt by the injected gas may cause solidification near the nozzle.

Bubble–liquid interfacial heat transfer

The heat flux from a bubble to the liquid phase (over a time interval of Δt) is given by

$$q'' = \frac{mc_p}{A_{int}\Delta t}(T_{b,2} - T_{b,1}), \qquad (11)$$

where $T_{b,2}$ and $T_{b,1}$ are the average bubble temperature at the end and the beginning of the time interval Δt as the bubble rises in the liquid medium. m and c_p are the bubble mass and specific heat, respectively, and A_{int} is the interface area. The gas interface and interface/liquid heat transfer coefficients $h_{int,g}$ and $h_{int,l}$ can now be defined as

$$q'' = h_{int,g}(T_b - T_{int}) = h_{int,l}(T_{int} - T_{liq}), \qquad (12)$$

where T_{int} is the interface temperature, introduced earlier in equation (8). However, no attempt was made to calculate the values of the heat transfer coefficients (from the present measurements) as the interface temperature T_{int} could not be measured accurately.

CONCLUSIONS

Measurement techniques were developed to study phase dispersion and phase resolved temperature distribution in gas–liquid two-phase flows. Electroresistivity probe and microthermocouple characteristics are analyzed in connection with the phase volume fraction, bubble frequency, bubble velocity, and phase resolved temperature measurements. Electroresistivity probe provides an easy and suitable tool to study phase volume fraction, bubble frequency and bubble velocity distributions. It was observed that the selection of the threshold voltage and sampling rate is not critical for the determination of the gas volume fraction and bubble frequency. A microthermocouple with a wire diameter of 25 μm together with a digital signal processing procedure is found to be satisfactory to obtain temperature distribution in each phase.

The local phase volume fraction, bubble frequency, bubble velocity, and phase resolved temperature distributions were experimentally studied in air sparged with water and multifluor inert fluid baths. The thermocouple signals were digitally filtered and compensated for the response time. The measurements were carried out to characterize the overall structure of the gas–liquid plume and the phase resolved temperature profiles.

The experimental measurements revealed that in the close proximity of the injection nozzle, the flow variables show steep changes in both radial and axial directions. With increasing axial distance, the profiles show a relatively uniform behavior in the axial as well as in the radial directions. The radial profiles of gas void fraction and bubble frequency at different axial locations exhibit good similarity, which can be approximated by a Gaussian distribution. The axial profiles of the gas temperature also show rapid decrease. The phrases reach thermal equilibrium within a short distance from the injection nozzle. However, for the experiments performed, close to the injection point, the gas temperature is considerably different from the liquid temperature.

The present measurements are of value in validating numerical models for the prediction of two-phase flows in gas injected liquid baths. Such measurements can provide a wealth of information for different combinations of gas/liquid systems. The phase resolved temperature measurements are of particular interest as they can be used for providing bubble/liquid heat transfer correlation. With detailed bubble velocity and gas–liquid interface temperature measurements, heat transfer coefficients on both sides of the interface can be determined.

REFERENCES

1. G. N. Oryall and J. K. Brimacombe, The physical behavior of gas jet injected horizontally into liquid metal, *Metall. Trans. B* **7**, 391–403 (1976).
2. K. H. Tacke, H. G. Schubert, D. J. Weber and K. Schwerdtfeger, Characteristics of round vertical gas bubble jets, *Metall. Trans. B* **16**, 263–275 (1985).
3. A. H. Castillejos and J. K. Brimacombe, Measurement of physical characteristics of bubbles in gas–liquid plumes: Part I. An improved electroresistivity probe technique, *Metall. Trans. B* **18**, 649–658 (1987).
4. A. H. Castillejos and J. K. Brimacombe, Measurement of physical characteristics of bubbles in gas–liquid plumes: Part II. Local properties of turbulent air–water plumes in vertically injected jets, *Metall. Trans. B* **18**, 659–971 (1987).
5. M. Sano and K. Mori, Dynamics of bubble swarms in liquid metals, *Trans. ISIJ* **20**, 668–674 (1980).
6. R. J. Andreini, J. S. Foster and R. W. Callen, Characterization of gas bubbles injected into molten metals under laminar flow conditions, *Metall. Trans. B* **8**, 625–631 (1977).
7. M. Kawakami, Y. Kitazawa, T. Nakamura, T. Miyake and K. Ito, Dispersion of bubbles in molten iron and the nitrogen transfer in the bubble dispersion zone at 1250°C, *Trans. ISIJ* **25**, 394–402 (1985).
8. S. Ohguchi and D. G. C. Robertson, Formation of porous accretions around tuyeres during gas injection, *Iron Steelmaking* **10**, 15–23 (1983).
9. A. A. Bustos, J. K. Brimacombe and G. G. Richards, Accretion growth at the tuyeres of a Peirce–Smith copper converter, *Can. Metall. Q.* **27**, 7–21 (1988).

10. C. Xu, Y. Sahai and R. I. L. Guthrie, Formation of thermal accretions in submerged gas injection process, *Ironmaking Steelmaking* **11**, 101–107 (1984).
11. S. K. Sharma, Criteria for predicting penetration of molten steel in tuyeres during inert gas injection, *Iron Steelmaker* **14**, 73–85 (1987).
12. O. C. Jones and J. M. Delhaye, Transient and statistical measurement techniques for two-phase flows: a critical review, *Int. J. Multiphase Flow* **3**, 89–116 (1976).
13. J. M. Delhaye, Local measurement techniques for statistical analysis. In *Handbook of Multiphase Systems* (Edited by G. Hetsroni), Chap. 10. Hemisphere, New York (1982).
14. G. F. Hewitt, *Measurement of Two-Phase Flow Parameters*. Academic Press, New York (1978).
15. A. Serizawa, I. Kataoka and Michyashi, Turbulence structure of air–water bubbly flow—I. Measuring techniques, *Int. J. Multiphase Flow* **2**, 221–233 (1975).
16. R. Van Der Welle, Void fraction, bubble velocity and bubble size in two-phase flow, *Int. J. Multiphase Flow* **11**, 317–345 (1985).
17. D. Barnea and L. Shemer, Void fraction measurements in vertical slug flow: applications to slug characteristics and transition, *Int. J. Multiphase Flow* **15**, 495–504 (1989).
18. A. H. Castillejos and J. K. Brimacombe, Physical characteristics of gas jets injected vertically upward into liquid metal, *Metall. Trans. B* **20**, 595–601 (1989).
19. R. A. Herringe and M. R. Davis, Structural development of gas–liquid mixture flows, *J. Fluid Mech.* **73**, 97–123 (1976).
20. N. Miller and R. E. Mitchie, Electrical probes for study of two-phase flows. In *Two-phase Flow Instrumentation* (Edited by B. W. Le Tourneau and A. E. Bergles), pp. 82–88. ASME, New York (1969).
21. S. A. Hinata, Study on the optimal fiber glass probe, *Bull. JSME* **15**, 1228–1235 (1972).
22. B. S. Shiralkar and R. T. Lahey, Diabatic local void fraction measurements in Freon-114 with hot-wire anemometer, *ANS Trans.* **15**, 880 (1972).
23. J. M. Delhaye, Hot-film anemometry in two-phase flows, *Proceedings of the Eleventh National Heat Transfer Conference* (1969).
24. B. D. Marcus and D. Dropkin, Measured temperature profiles within the superheated boundary layer above a horizontal surface in saturated nucleate pool boiling of water, *J. Heat Transfer C* **87**, 333–341 (1965).
25. S. J. D. Van Stralen and W. M. Sluyter, Local temperature fluctuations in saturated pool boiling of pure liquids and binary mixtures, *Int. J. Heat Mass Transfer* **12**, 187–198 (1969).
26. N. Stefanovic, N. Afgan, V. Pislar and L. J. Jovanovic, Experimental investigation of the superheated boundary in forced and convection boiling. In *Heat Transfer* Vol. 5. Elsevier, Amsterdam (1970).
27. N. Afgan, L. J. Jovanovic, M. Stefanovic and V. Pislar, An approach to the analysis temperature fluctuation in two-phase flow, *Int. J. Heat Mass Transfer* **16**, 187–194 (1973).
28. J. R. Wiebe and R. L. Judd, Superheat layer thickness measurements in saturated and subcooled nucleate boiling, *J. Heat Transfer* **94**, 455–461 (1971).
29. H. Turkoglu, Transport process in gas injected liquid baths, Ph.D. thesis, Drexel University, Philadelphia, PA (1991).
30. A. Castillejos, A study of the fluid-dynamic characteristics of turbulent gas–liquid bubble plumes, Ph.D. thesis, The University of British Columbia (1986).
31. Y. Iida, Study of local void fraction, *J. Atom Energy Soc. Jap.* **14**, 337–339 (1972).
32. J. Bendat and A. Piersol, *Random Data: Analysis and Measurement Procedure*, pp. 296–299. Wiley, New York (1971).
33. D. Bradly, A. K. C. Lau and M. Missaghi, Response of compensated thermocouples to fluctuating temperatures: computer simulation, experimental results and mathematical modeling, *Combust. Sci. Technol.* **64**, 119–134 (1989).
34. S. F. Son, M. Queiroz and C. G. Wood, Compensation of thermocouples for thermal inertia effects using a digital deconvolution, *ASME Proceedings of National Heat Transfer Conference*, August, HTD-Vol. 106, pp. 515–522 (1989).
35. L. L. Moresco and E. Marschall, Temperature measurements in a liquid–liquid direct-contact heat exchanger, *AIChE Symp. Ser.* **75**, 266–272 (1980).
36. W. V. Heito, A. M. K. P. Taylor and J. H. Whitelaw, Simultaneous velocity and temperature measurements in premixed flames, *Expl Fluids* **3**, 323–339 (1985).
37. A. Yoshida, Structure of opposed jet premixed flame, *Presented at the Twenty-second International Symposium on Combustion*, The Combustion Institute, Seattle, WA, paper no. 152 (1988).
38. P. Cambray, M. Vachon, T. Maciaszed and J. C. Bellet, Instantaneous compensation of fine wire thermocouple inertia in a buoyant turbulent diffusion flame, *The 23rd ASME National Heat Transfer Conference*, Denver, CO (1985).
39. F. C. Lockwood and H. Moneib, Fluctuating temperature measurements in a heated round free jet, *Combust. Sci. Technol.* **22**, 63–81 (1980).
40. A. J. Yule, D. S. Taylor and N. A. Chingier, On-line digital compensation and processing of thermocouples signals for temperature measurements in turbulent flames, *AIAA Sixteenth Aerospace Science Meeting* (1978).
41. H. L. Ozem and F. C. Goudin, Temperature time series measurement in premixed V-shaped flames, *Eastern States (Combustion Institute) Meeting*, November pp. 36:1–36:4 (1989).
42. W. E. Ranz and W. R. Marshall, Evaporation from drops, *Chem. Engng Prog.* **48**, 141–146 and 173–180 (1953).